

Sweat-Permeable, Biodegradable, Transparent and Self-powered Chitosan-Based Electronic Skin with Ultrathin Elastic Gold Nanofibers

Xiao Peng, Kai Dong, Yufei Zhang, Lili Wang, Chuanhui Wei, Tianmei Lv,
 Zhong Lin Wang,* and Zhiyi Wu*

The simultaneous achievement of multiple functional attributes, such as flexibility, stretchability, transparency, comfortability, biodegradability, and self-powered ability into electronic skins (e-skins) is vital to their long-term practical applications. Due to the internal contradiction between functional material combination and simple structural design, this kind of multifunctional e-skin has rarely been fabricated or even reported. To this end, chitosan (CS), a natural material with remarkable biocompatibility, biodegradability, and electron-donating ability, is integrated with a single-mode triboelectric nanogenerator (TENG) to develop a multifunctional e-skin, which includes sweat permeability, controllable biodegradability, high transparency, and self-powered sensing ability. In addition, a facile, efficient, and large-scale fabrication strategy is proposed to construct stretchable, ultrathin, transparent, and shape-adaptable gold nanofibers (Au NFs) electrodes. Furthermore, the e-skin can achieve a voltage response pressure sensitivity of 0.012 kPa^{-1} in the pressure range of 0–70 kPa and a fast response time of 70 ms. Finally, it shows controllable and excellent degradability in various solutions. It is believed that the proposed e-skin based on the design and integration of CS and Au NFs will provide a paradigm shift for the next-generation self-powered transient electronics.

1. Introduction

Human skin is one of the largest organs covering the whole body and plays an important role in regulating our interac-

tions with the external world.^[1] Inspired by the functions and characteristics of human skin, electronic skin (e-skin) represents one of the mainstream innovations, providing the possibility to reproduce or even surpass the properties of real skin, which has a far-reaching influence on non-invasive healthcare systems,^[2,3] human-machine interfacing devices,^[4,5] artificial intelligence, and prosthetics.^[6–8] In order to mimic the ultra-sensitive self-perception ability of natural skin, e-skins require a sufficient external power supply to respond to various external stimuli, such as humidity, temperature, pressure, and so on.^[9] However, the power supplying issue of limited power or frequent charging limits the extended application of e-skins in time and space scales. Fortunately, self-powered devices provide an alternative strategy to this issue.^[10–12] At present, several types of electromechanical conversion principles, including capacitance,^[13,14] piezoresistance,^[15] piezoelectricity,^[16] and triboelectricity,^[17–19] are often

employed to provide the electrical signal for e-skins. Particularly, as an emerging technology for energy harvesting and self-powered sensing, triboelectric nanogenerator (TENG) has the advantages of simple structure, easy to fabricate, and diverse

X. Peng, K. Dong, Y. Zhang, C. Wei, T. Lv, Z. L. Wang, Z. Wu
 Beijing Institute of Nanoenergy and Nanosystems
 Chinese Academy of Sciences
 Beijing 100083, P. R. China
 E-mail: zhong.wang@mse.gatech.edu; wuzhiyi@binn.cas.cn

X. Peng, K. Dong, Y. Zhang, C. Wei, Z. L. Wang, Z. Wu
 College of Nanoscience and Technology
 University of Chinese Academy of Sciences
 Beijing 100049, P. R. China

L. Wang
 State Key Laboratory for Superlattices and Microstructures Institute of Semiconductors
 Chinese Academy of Sciences
 Beijing 100083, P. R. China

T. Lv
 School of Chemistry and Chemical Engineering
 Guangxi University
 Nanning 530004, P. R. China

Z. L. Wang, Z. Wu
 CUSPEA Institute of Technology
 Wenzhou, Zhejiang 325024, P. R. China

Z. L. Wang
 School of Materials Science and Engineering
 Georgia Institute of Technology
 Atlanta, GA 30332, USA

 The ORCID identification number(s) for the author(s) of this article can be found under <https://doi.org/10.1002/adfm.202112241>.

DOI: [10.1002/adfm.202112241](https://doi.org/10.1002/adfm.202112241)

material options, which enables to convert of ubiquitous mechanical energy into an electrical signal.^[20–24] Therefore, the integration of versatile TENG technology into functional e-skins brings new vitality and more possibilities for the next generation of wearable electronic products, personal healthcare, and human-machine interaction systems.^[4]

The pursuit of e-skin has inspired material innovation to imitate the unique characteristics of the skin, including stretchability, mechanical durability, biodegradability, and breathability.^[25] Traditional plastic or elastomer substrates, such as polyethylene terephthalate (PET), polydimethylsiloxane (PDMS), and polyimide (PI), greatly limit their practical applications and long-term feasibility because of mechanical mismatch, limited degradability, impermeability, and discomfort.^[26–28] Therefore, advanced materials derived from renewable and sustainable biomass, such as polysaccharides (cellulose, chitin, chitosan, starch) and protein (silk, gelatin), have attracted great attention because of their nonpetroleum sources, environmental friendliness, and carbon neutrality, which make them expected to be the substitutes for green and degradable substrates in flexible electronics.^[29–31] As a natural, biocompatible, and biodegradable polymer, chitosan (CS) is the deacetylation product of chitin, the second largest natural polymer after cellulose.^[32] CS is considered one of the most valuable natural polymers because of its valuable inherent characteristics, such as antibacterial, antifungal, antiviral, nontoxic, completely biocompatible, and biodegradable, as well as film-forming, fiber-forming, and hydrogel-forming properties.^[33] By virtue of these characteristics, CS has potential applications prospects in many fields such as food, agriculture, medicine, cosmetics, water treatment, pulp and paper making, textile industry, and so on.^[34] In addition, CS-based membranes have been widely studied in the medical industry due to their potential in the development of artificial skin.^[35,36] Besides, controllable degradation, high transparency, and favorable membrane forming properties make CS membrane have great potential applications in flexible, transparent, and transient wearable electronic devices.^[37] However, the application of pure CS membrane in e-skin remains a significant challenge due to its unsatisfactory mechanical properties and bad water vapor penetration ability.^[38]

Another vital component for e-skin is the epidermal electrode that should possess metallic conductivity, ultrathin thickness, high stretchability, facile pattern ability, transparency, and breathability for practical applications. However, it is greatly challenging to achieve these characteristics simultaneously.^[39,40] Typically, there are trade-offs between these properties. And it is difficult to achieve these goals at the same time. Most electrodes of e-skins are membranes formed by spray-coating, evaporation, or sputtering, which lack ductility, air permeability, and transparency.^[41] Prestraining or geometric engineering approaches, including the use of buckled metal thin films or serpentine metal interconnects, are rendered mechanically stable of conductors, but they are not suitable for large-scale production.^[42] Intrinsically conducting polymers and ionic conductors consisting of hydrogels and conductive ions have attracted much attention due to their high stretchability and transparency.^[43,44] However, these conductors have low conductivity or fluidity of a liquid, providing a huge challenge to the electrode pattern and device packaging. In addition, metal nanowires,^[45] carbon

nanotubes,^[46] graphenes,^[17,40] and MXene^[47–49] have been widely used to prepare electrodes by doping, spin coating, or dip coating, but their conductivity and transparency are difficult to control, and the substrate is limited by the type of conductive dispersion solvent. Recently, networked metallic nanofibers have the advantages of high stretchability and high transparency, excellent biocompatibility, and favorable water-air permeability due to the continuity of nanofibers, large surface area, and numerous micro-nano holes, which have broad application potential in wearable electronics.^[50–52]

Here, a multifunctional e-skin is demonstrated by exploiting micro-crack structured CS membranes as the dielectric layer and substrate and interlaced gold nanofibers (Au NFs) as the intermediate electrode. In our e-skin, the CS membrane is realized through an all green, facile, and readily implementable casting method. It has excellent optical transparency (94.8%), good flexibility (87% elongation, Young's modulus of 1.3 MPa), high sweat vapor permeability (water vapor transmission rate of $1.91 \text{ kg m}^{-2} \text{ d}^{-1}$), and remarkable degradability. In addition, the Au NFs electrode is prepared by simple operation and convenient large-scale preparation methods, including electrospinning, magnetron sputtering, and photolithography, making it highly transparent, ultra-thin, stretchable, highly conductive, breathable, and pattern designable. Besides, the TENG-based e-skin can achieve self-powered sensing in the pressure range from 0 to 70 kPa, with a voltage response pressure sensitivity of 0.012 kPa^{-1} and a fast response time of 70 ms. In addition, it can be completely and controllably decomposed through a series of degradation reactions in various degradation solutions (including acid, enzyme, and hydrogen peroxide). Due to the aforementioned excellent performance, our e-skin is an ideal choice for green electronic products in biomedical devices, human-machine interfaces, and virtual or augmented reality devices.

2. Results and Discussion

2.1. Fabrication and Characterization of CS Membrane

To improve the practicability of e-skins, flexibility, permeability, biocompatibility, and imperceptibility are highly desirable features. **Figure 1a** illustrates the fabrication procedure of the transparent, flexible, and permeable CS membrane. Briefly, by dissolving CS powder in acetic acid, and then removing impurities by centrifugation, a stable and homogeneous CS solution is obtained at first. Subsequently, the membrane is obtained by solution casting and can be easily peeled off from the substrate. Details can be seen in the Experimental Section. Due to the di-equatorial glycosidic linkage in the CS structure, pure CS membrane has the characteristics of poor tensile property and gas penetration ability, which limits its application in e-skins. To address this issue, plasticizers such as glycerol are usually added to the membranes to improve flexibility, chain fluidity, gas exchange, and water vapor transmission performance. It is worth noting that compared with other additives, glycerol is a colorless, odorless, and viscous liquid, which is nontoxic and safe for the human body. As shown in **Figure 1b**, it is obvious that the obtained CS membrane can be flexible and foldable.

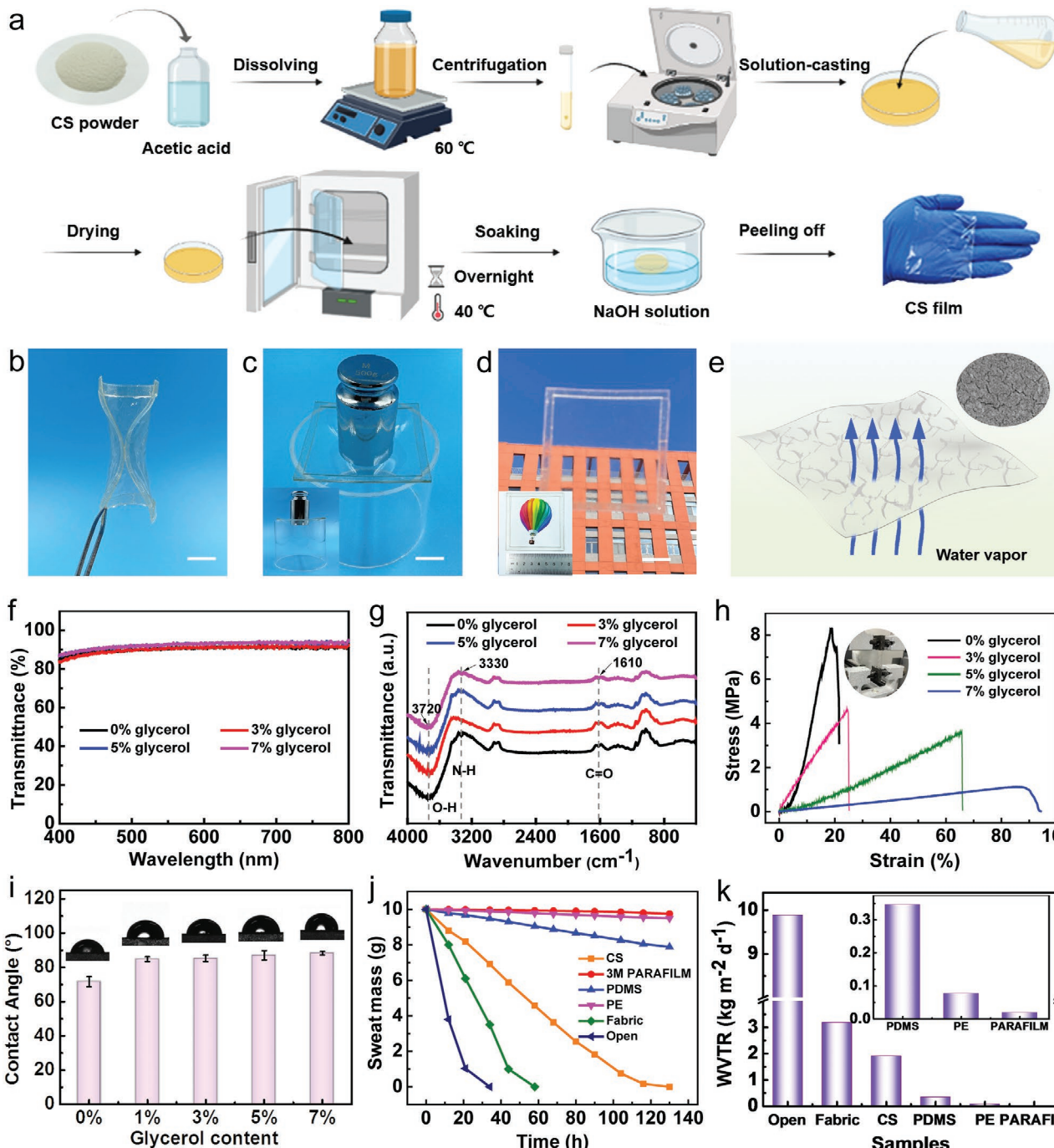


Figure 1. Fabrication process and properties of chitosan membrane. a) Schematic illustration of the fabrication process of CS membrane. b) The flexibility of the CS membrane. Scale bar: 1 cm. c) Top view and front view (inset) of the CS membrane under 500 g load. Scale bar: 1 cm. d) Digital photos of the transparent CS membrane outdoors and indoors (inset). Scale bar: 1 cm. e) The diagram of the micro-crack structure of CS membrane. Inset: SEM image of CS surface. f) The transmittance of the CS membranes with different content of glycerol. g) FTIR of the CS membranes with different content of glycerol. h) Strain-stress curves of the CS membranes with different content of glycerol. i) Water contact angle of the CS membranes with different content of glycerol. Error bars represent the SD ($n = 3$, $p < 0.05$). j) Sweat vapor permeability test of CS membrane, commercial 3M sealing membrane, PDMS, PE, fabric, and open status at 37 °C and 40% RH. k) Water vapor transmittance rates (WVTRs) of CS membrane, commercial 3M sealing membrane, PDMS, PE, fabric, and open status at 37 °C and 40% RH.

Moreover, Figure 1c shows typical images of the CS membrane with a thickness of 20 μm extending without breaking under the pressure of 500 g, in which the weight of the load

is 5000 times that of the CS membrane (0.1 g), which proves its great pliability and tenacity. In addition, it exhibits high transparency indoors or outdoors (Figure 1d). As a result of

acid neutralization and water evaporation during the process, the micro-crack structure of the CS membrane with the width of $0.032 \pm 0.007 \mu\text{m}$ can be observed by SEM image, thus providing moisture flow channels between human skin and the external environment (Figure 1e).

The UV-vis spectrum curves of CS membranes with different content of glycerol demonstrate a high transmittance of more than 83% in the visible light range, in which the transparency of the CS membrane with 7% glycerol can reach 94.8% at 800 nm (Figure 1f). Furthermore, the changes of chemical and aggregated structures of the pure CS and CS/glycerol membranes are analyzed. The FTIR spectra of the obtained membrane complexes show that the peaks at 3720, 3330, and 1140 cm^{-1} are attributed to the hydroxyl group (O–H), amide group (N–H), and carbonyl group (C=O) stretching vibrations of CS, respectively (Figure 1g). In the case of CS treated with glycerol, the same bonds can be observed in spectra of CS/glycerol membranes, indicating that CS retains its chemical structure. X-ray diffraction (XRD) analysis shows two strong diffraction characteristic peaks around 2θ of 11° and 20° , corresponding to crystals I and II of CS, respectively (Figure S1, Supporting Information). This is due to the strong H-bonding effect in and between the chitosan molecules, which produces a certain rigidity of the chitosan molecular chain, leading to the formation of a certain crystalline state. XRD and FTIR results indicate that when the glycerol content is <7%, the crystallinity and molecular structure of the chitosan are not affected. The mechanical properties of the CS membrane can be tuned by adjusting the content of glycerol. Figure 1h shows the typical stress-strain curves for CS membranes with different CS/glycerol volume ratios (0%, 3%, 5%, and 7%). As the increase of glycerol content, Young's modulus decreases. This is because the addition of glycerol can reduce the intermolecular forces and increase the mobility of the biopolymer chain, thereby resulting in a much softer and stretchable membrane, which is suitable for the e-skin application. Notably, the elongation of the membrane can reach 87%, and Young's modulus is 1.3 MPa (on average, biological skin can be stretched to 75% strain,^[8] and Young's modulus of human skin is 0.14–0.6 MPa^[53]), indicating that its mechanical properties are comparable to those of epidermis. Because the hydrogen bond between CS and glycerol hinders the diffusion of water molecules, glycerol increases the contact angle of the CS membrane from 71.6° to 88.2° , making the CS membrane much more hydrophobic (Figure 1i), which is essential for CS membrane in e-skin as the substrate layer to protect water from diffusing to the electrode.

Sweat accumulated in human skin could cause physical sensor malfunction or skin discomfort. Therefore, e-skin with sweat permeability is very necessary for long-term use. The amount of sweat water loss of different covers (CS membrane, commercial 3M sealing membrane, PDMS, PE, fabric, and open state) is recorded (Figure 1j and Experimental Section). Figure 1k shows the estimated sweat water vapor transmission rate (WVTR) of various membranes, which indicates that the WVTR of CS membrane ($1.91 \text{ kg m}^{-2} \text{ d}^{-1}$) is comparable to that of common cotton fabric ($3.18 \text{ kg m}^{-2} \text{ d}^{-1}$) and much superior to that of PDMS ($0.35 \text{ kg m}^{-2} \text{ d}^{-1}$), PE membrane ($0.076 \text{ kg m}^{-2} \text{ d}^{-1}$) and commercial 3M sealing film ($0.019 \text{ kg m}^{-2} \text{ d}^{-1}$). The high WVTR can accelerate perspiration evaporation of sweat, improve

user comfort, and minimize inflammation caused by sweat accumulation. It is well known that permeability is related to the surface morphology of the samples. Because there are numerous voids between yarns in the fabric, the WVTR is higher. SEM images of the membranes (CS membrane, commercial 3M sealing membrane, PDMS, PE) further confirm that the obvious micro-cracks in CS membrane contribute to the transfer of sweat vapor molecules (Figure S2, Supporting Information), showing its great application prospects in wearable skin electronics.

2.2. Fabrication and Characterization of Au NFs Electrode

E-skin is a group of epidermal electronic devices, in which one of the vital components is the ultrathin elastic conductor. Its mechanical compliance, good electrical performance, and compatibility with large-area processing techniques are very important to manufacture highly functional devices. Here, we present a method with simple operation and easy large-scale production to fabricate stretchable, ultrathin, breathable, and patterned Au nanofibers (Au NFs) electrodes. Figure 2a presents schematic illustrations that describe the fabrication of CS/Au NFs/CS electronic skin. It consists of four steps, including metallization, nanofiber mesh transfer, patterning, and packaging. First, a nanofiber mesh made of biocompatible polyvinyl alcohol (PVA) is fabricated by electrospinning. Metallization of PVA nanofibers is then carried out by magnetron sputtering to deposit a thin layer of gold on the surface of the PVA nanofibers. Using this process, large-scale Au NFs with excellent electrical conductivity are obtained. It is worth noting that this process can be applied to various metal materials, including gold, silver, copper, and platinum. Then, photolithography technique and wet etching are employed to obtain the patterned Au NFs electrode. After exposure and development, the uncovered Au NFs are chemically etched with the aqua regia immediately, and the residual photoresist is then removed by acetone. Finally, the patterned Au NFs electrode is encapsulated into the electronic skin device using thin CS membranes. More detailed information can be found in the Experimental Section.

The CS/Au NFs membrane can directly contact human skin, as shown in Figure 2b. The hair and blood vessels of the hand under the membrane can be clearly seen with the naked eye, showing its high transparency, flexibility, and conformality (Figure S3, Supporting Information). For demonstration, the figure of the butterfly (Figure 2c; Figure S4, Supporting Information) composed of Au NFs are fabricated on CS substrate, in which the clear edge of the Au NFs can be observed. Meanwhile, this figure shows high optical transparency. This method is suitable for preparing electrodes with various transparent and conductive patterns, which can be transferred to various substrates, such as a wafer, plastic substrates, or even elastomeric substrates for further processing. Therefore, it has broad application prospects in personalized, customized, and imperceptible electronic devices. Figure 2d,e shows the plane and cross-sectional SEM images of the smooth and continuous Au NFs, respectively, with a diameter of $891 \pm 202 \text{ nm}$ and a thickness of several microns. The multilayer interlaced Au NFs networks and numerous 3D micro/nanopores provide high light transmittance and multiple thermal-moisture transfer

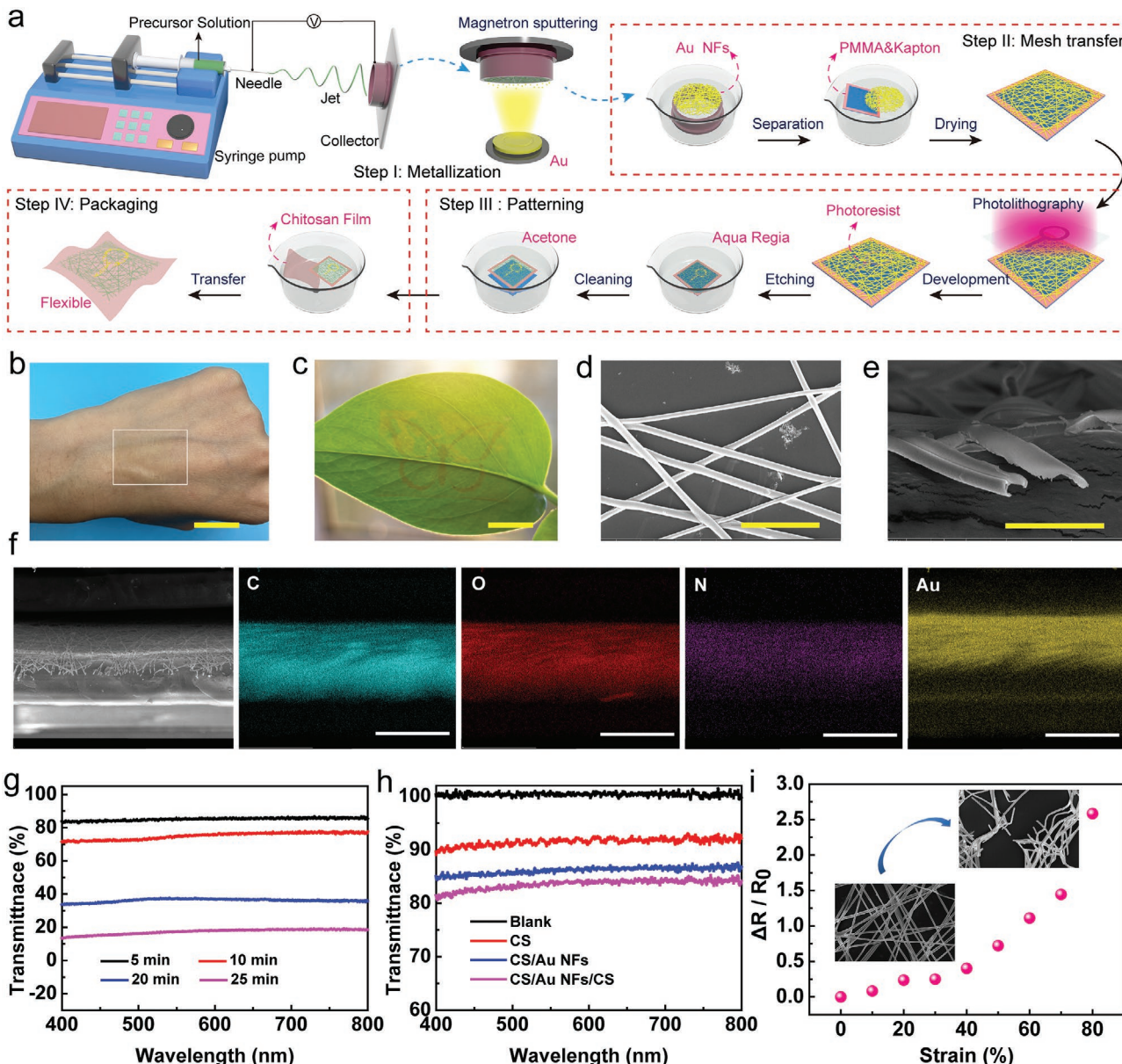


Figure 2. Fabrication and characterization of the CS/Au NFs/CS e-skin with Au NFs electrodes. a) Schematic illustration of the fabrication process of Au NFs and the e-skin device. b) Digital photo of CS/Au NFs on the back of the hand, marked with a white box. Scale bar: 1 cm. c) Picture of butterfly with patterned Au NFs electrode on CS membrane placed on the leaf. Scale bar: 2 cm. d,e) SEM images of Au NFs in plane (d) and cross-section (e). Scale bar: 10 μ m and 3 μ m, respectively. f) Cross-section morphology and EDS of CS membrane with Au NFs. Scale bar: 50 μ m. g) Transparency of the Au NFs with electrospinning duration of 5, 10, 20, and 25 min, respectively. h) Transparency of the CS membrane, CS/Au NFs, and CS/Au NFs/CS. i) Strain-dependent resistance changing rate of Au NFs. Insets: SEM images of initial status and 80% strain, respectively.

channels, making them highly conductive, transparent, and breathable. The corresponding energy-dispersive X-ray spectroscopy (EDX) elemental mappings confirm that Au NFs electrode adheres well to the surface of the CS membrane (Figure 2f).

The optical transparency of the Au NFs electrodes and the e-skin are also investigated by analyzing UV-vis spectroscopy spectra. As shown in Figure 2g, with the increase of electrospinning time, denser nanofibers can be obtained, resulting in the decrease of optical transparency. The Au NFs electrode can reach 86% transmittance when the electrospinning time is 5 min, demonstrating excellent performance as a transparent

conductive electrode. Due to the high optical transparency of CS substrate (94.8%) and Au NFs electrode (86%), the CS/Au NFs/CS e-skin shows transmittance of 84% at a wavelength of 800 nm (Figure 2h).

Further tests are carried out to demonstrate the conductivity and stretchability of the Au NFs electrodes. The relative change in resistance, $\Delta R/R_0 = (R-R_0)/R_0$, is usually used to evaluate the change of conductance under specific strains. Figure 2i presents the resistance change of the multidirectional random Au NFs electrodes under different tensile strains. It can be found that the larger the tensile strain, the greater the resistance. It is worth

noting that the resistance remains in a very small variation range, and it even exhibits a sheet resistance of $25.8 \Omega \text{ sq}^{-1}$ at 80% strain value (Figure S5, Supporting Information). With the increase of tensile strain, the staggered Au NFs are oriented along the tensile direction and gradually form fractures (Figures S6 and S7, Supporting Information), which renders the conductivity of Au NFs electrode decrease. Additionally, the variation of Au NFs network under different tensile strains is further confirmed via the finite element analysis method (Figure S8, Supporting Information), indicating that the electrode edges along the stretching direction have greater stress. All these results reveal that the Au NFs electrode has strain-insensitive conductance, which is conducive to its practical applications in wearable electronics.

2.3. Electrical Output and Sensing Performance

CS/Au NFs/CS e-skin with a sandwich structured of $10 \mu\text{m}$ in thickness works in a single-electrode mode of TENG, and its

working principle is the coupling effect of contact electrification and electrostatic induction. The electricity generation and transmission mechanism of the TENG-based e-skin are illustrated in Figure 3a, which is realized by the periodic contact and separation movements between the e-skin and its contact object. Take human skin as the contact material, when the skin contacts the CS membrane, electrification occurs at the interface, and the same amount of charges with opposite polarities are generated on the surface of the skin and CS membrane (Figure 3a(i)). When the two surfaces separate, the static charges on the surface of the CS membrane induce the movement of electrons in the Au NFs electrode to balance them, generating an instantaneous electrical current (Figure 3a(ii)). When the skin and CS membrane are completely separated, the negative charges in the top CS layer are fully equilibrated by the electrostatic induced charges on the Au NFs electrode, reflecting the neutralization of positive and negative charges in this period (Figure 3a(iii)). In the reverse case, if the skin is approaching back to the e-skin the accumulated positive charges in top Au NFs flow back to

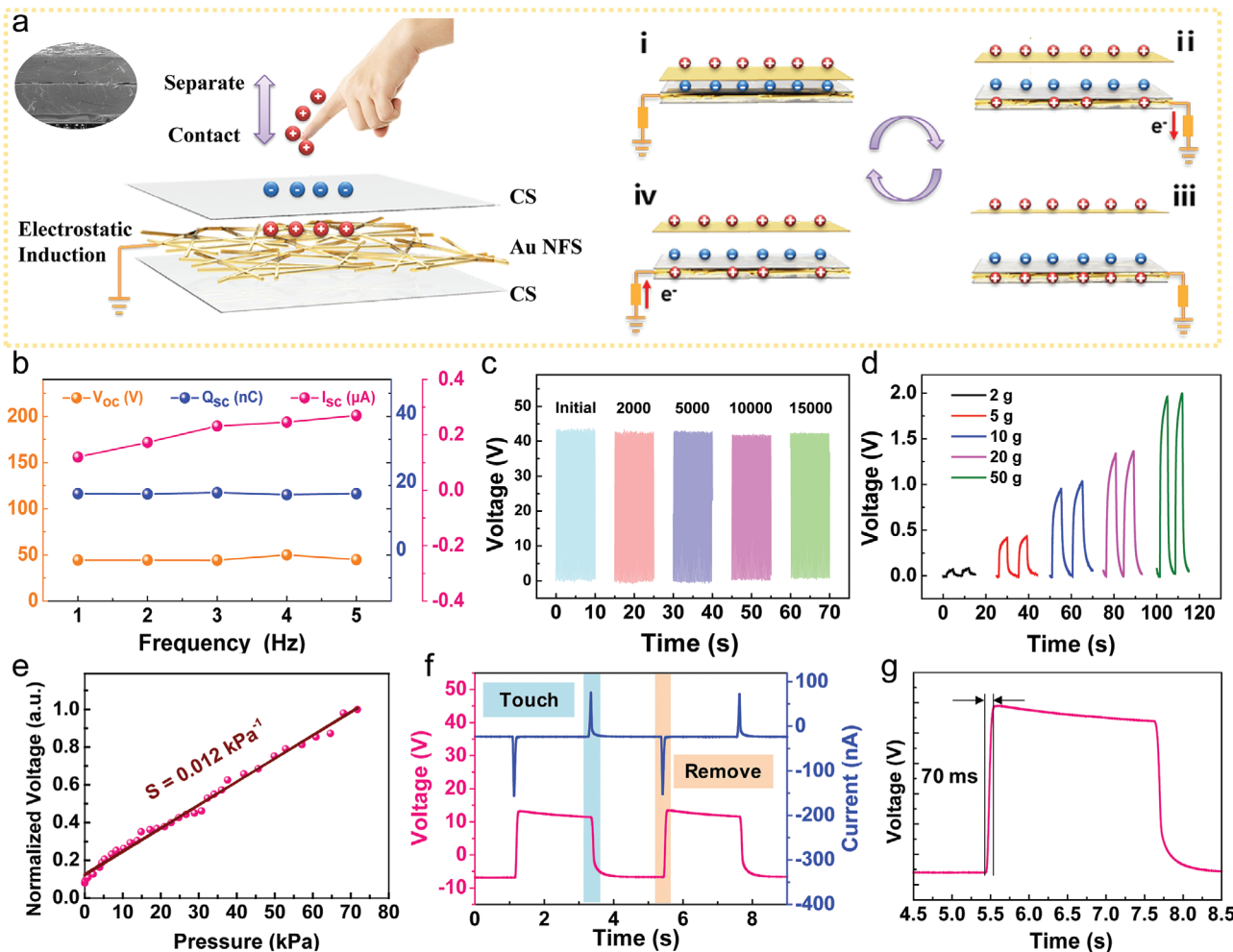


Figure 3. Electrical and sensing performances of the CS/Au NFs/CS e-skin. a) Schematic illustration of the working mechanism of the e-skin is a complete contact-separation cycle, including i) fully contact, ii) gradually separating, iii) fully separated, and iv) gradually approaching. Upper left inset: SEM image of a cross section of the e-skin. b) Frequency-response characteristics of the e-skin under different loading frequencies (1–5 Hz), including V_{oc} , I_{sc} , and Q_{sc} . c) Stability of the e-skin under 15 000 cycles. d) Voltage response to weights of different masses, including 2, 5, 10, 20, and 50 g, respectively. e) Voltage response to a wide range of pressures (0–70 kPa). f) Output voltage and current signal of the e-skin under cyclic touch process. g) Response time of the e-skin.

the ground through the external load to compensate for electrical potential differences (Figure 3a(iv)). After the whole system returns to the initial state, the negative charges on the CS are fully offset by the positive charges on the external skin again (Figure 3a(i)). As a result, a contact-separation process between human skin and the e-skin will generate an instantaneous alternating potential and current through the external load. To obtain a more quantitative understanding of the electricity generating process, a theoretical model of the e-skin is established to observe the electric potential distribution of every component under the fully separated state by a simple finite element simulation using COMSOL Multiphysics (Figure S9, Supporting Information).

To quantitatively assess the electrical output performance of the e-skin, the indicators, including open-circuit voltage (V_{OC}), short-circuit current (I_{SC}), and short-circuit charge transfer (Q_{SC}), is measured by a mechanical linear motor with a frequency of 1–5 Hz. For details, please refer to the Experimental Section and Figure S10 (Supporting Information). As shown in Figure 3b, V_{OC} and Q_{SC} almost remain constant (45 V and 16 nC, respectively), while a gradually increasing I_{SC} (from 0.12 to 0.27 μ A) is observed as the frequencies increase from 1 to 5 Hz under a load of 8 N (Figure S11, Supporting Information). The potential reason can be attributed that V_{OC} and Q_{SC} are independent of speed, which means that the variation of movement frequency will cause no change of the V_{OC} and Q_{SC} . However, the I_{SC} depends on the relative movement speed, which presents a positive correlation feature with the increase of speed (Note S1, Supporting Information). Working stability is vital for e-skin. After 15 000 cycles of continuous loading, V_{OC} has no obvious attenuation, which proves that it has excellent stability and durability for long-term use (Figure 3c). Therefore, our e-skin has wide application potential in the field of wearable electronic products and self-powered sensing.

To further study the sensing performance of the e-skin, weights with different masses are applied to the e-skin, which indicates that the output voltage increases with the increase of load (Figure 3d). The pressure sensitivity of the e-skin as a function of loading pressure is also investigated, which is defined as, $S = d(\Delta V/V)/dP$, where ΔV is the relative change in voltage, V is the saturation voltage, and P is the applied pressure. The normalized voltage is almost linearly related to the pressure from 0 to 70 kPa, where the pressure sensitivity is 0.012 kPa⁻¹, that is, the corresponding slope of the curve (Figure 3e). The response time of the designed e-skin is estimated by loading and unloading cycles at a load of 5 N. When pressure is applied to the e-skin, an instantaneous change of I_{SC} and V_{OC} occurs (Figure 3f). The fast response time of our device is 70 ms as illustrated in Figure 3g, which is calculated based on the response of full-scale voltage to the applied pressure. The high sensitivity and fast response time of the e-skin make them suitable for detecting minute pressure changes.

2.4. Degradable Performance

Considering the safety and environmental friendliness of flexible wearable sensors, biodegradable electronics have attracted extensive attention in disposable wearable patch-type sensors

and implantable medical devices. Biodegradability refers to the ability to partially or completely degrade, dissolve, or disintegrate in an actively or passively controlled way under certain conditions. In order to evaluate the biodegradability of our e-skin, *in vitro* biodegradation studies have been conducted. The device can be immersed in various media, such as acid solution, hydrogen peroxide solution, enzyme solution, etc., showing its extensive and excellent degradability (Figure 4a). Since chitosan is a natural polysaccharide composed of 2-acetamido-D-glucose and 2-amino-D-glucose units linked with glycosidic linkages, as shown in Figure 4b, which are susceptible to degrade and decompose into oligomers during the degradation process. For comparison, degradation performances of CS and CS/Au NFs membranes within 30 h are studied, and their photo changes in the corresponding degradation cycle are recorded. The results show that after 15 min, the CS membrane first shrinks rapidly, then it is hydrolyzed by acid and degraded in bulk. In addition, after soaking in acetic acid at room temperature for 1 h, it almost completely disappears (Figure S12, Supporting Information). In pepsase aqueous solution, the CS membrane gradually changes from transparent to yellow and totally degrades after incubation at 37 °C for 30 h. Besides acid degradation and enzyme degradation, oxidative degradation is also an effective way to decompose CS. It is found that CS membrane shrinks slightly after 1 h in hydrogen peroxide (H_2O_2) aqueous solution, and completely disappears after 30 h. In contrast, the degradation period of the CS/Au NFs membrane in acid solution is much longer, because the presence of Au NFs improves the anti-permeability ability (Figure 4c; Figure S13, Supporting Information). This can also be confirmed in other degradation solutions. The CS/Au NFs membrane maintains a stable morphology at the initial stage (Figure 4d,e). Then, CS/Au NFs are hydrolyzed by water absorption, which is the same as the degradation process in the CS membrane. It should be noted that the gold electrode cannot be degraded and disintegrated in the solution, so it will be dispersed in the solution as gold particles. However, this does not hinder the degradability of our e-skin, because biodegradable electronic products can be divided into partial degradation and complete degradation.^[54] In order to make the e-skin completely biodegradable, dissolvable metals (Mg, Fe, etc.) may be good choices. However, the processability, stretchability, and transparency of metalized nanofibers need further study.

3. Conclusions

In summary, we have developed a multifunctional CS/Au NFs/CS e-skin based on TENG, which integrates high transparency, good flexibility, remarkable sweat vapor permeability, excellent biodegradability, inherent antibacterial property, and energy autonomy. The CS membrane is prepared by a green and easy solution-casting method. The flexibility, hydrophobicity, and water vapor permeability of the membrane are improved by adding glycerol. Besides, taking advantage of large-specific surface area and numerous micro/nano-pores structures of interlaced nanofiber networks, ultrathin, transparent, flexible, stretchable, breathable, and high-resolution patterned Au NFs electrode is fabricated by readily implementable and scalable

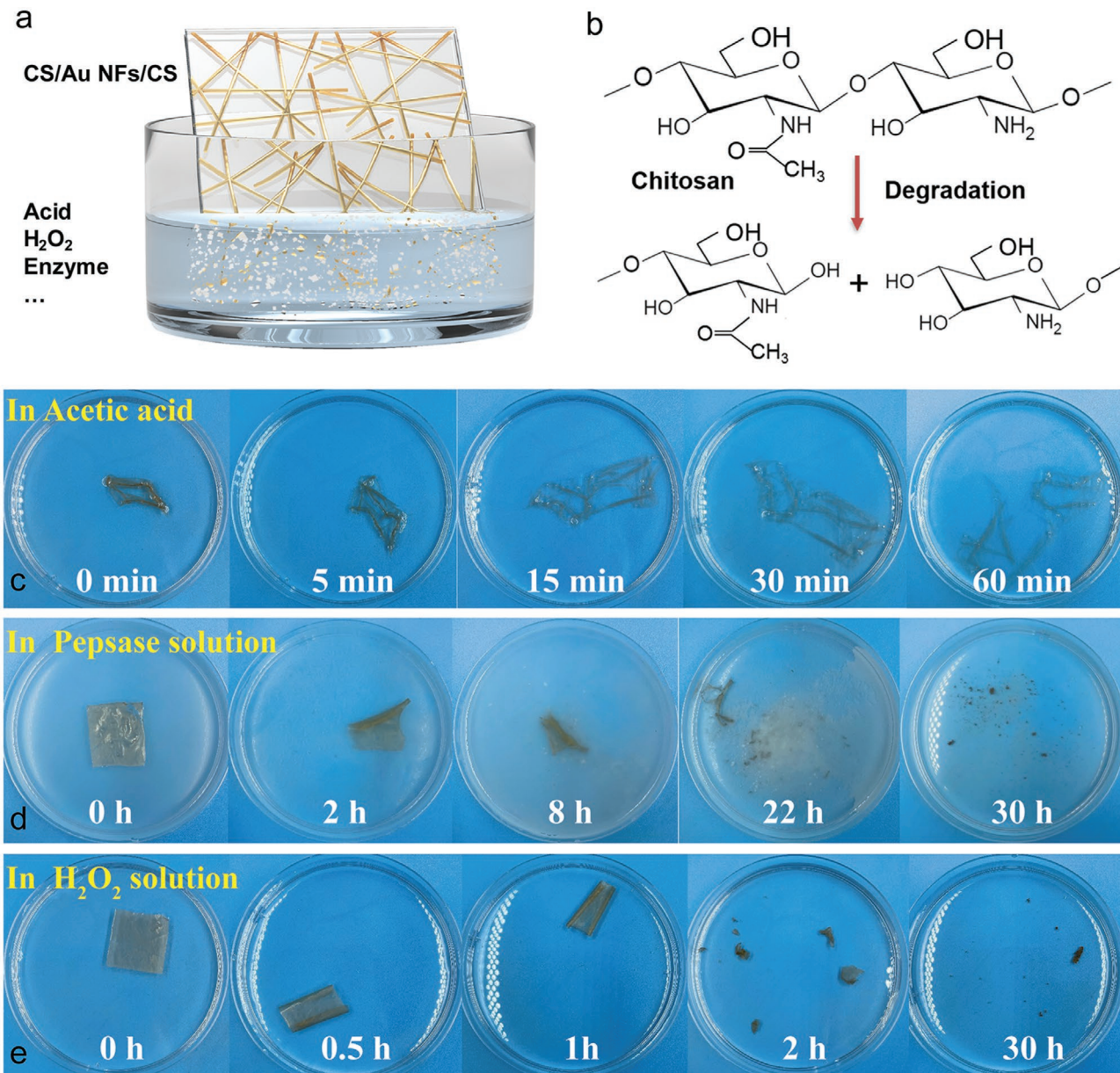


Figure 4. Degradation performance of the e-skin. a) Schematic diagram of the biodegradable e-skin under various conditions. b) Degradation mechanism of the CS. c–e) Sequential photographs of CS/Au NFs membrane biodegradation in vitro, that is, photos in (c) acetic acid, (d) pepsase solution, and (e) hydrogen peroxide solution.

methods, including electrospinning, magnetron sputtering and photolithography. In addition, the e-skin based on the single electrode mode TENG has a voltage response pressure sensitivity of 0.012 kPa^{-1} and a fast response time of 70 ms, which are both relatively high (Table S1, Supporting information). Moreover, it can be degraded rapidly, easily, and controllably by various solutions. Therefore, sensitive perception functionality and basic practical features are well integrated into our designed e-skin. Although some aspects of the e-skin need to be further optimized and improved, such as the potential impact of pollutants. However, our study still broadens the application fields of e-skin, such as green electronics, transparent devices, and comfortable wearable products due to its excellent practicabilities,

such as environmental friendliness, high transparency, and sweat permeability.

4. Experimental Section

Fabrication of TENG-Based E-Skin: i) Fabrication of CS membrane: a mixture of the desired amount of CS powder (molecular weight, 100 000) and a defined amount of glycerol (1%, 3%, 5%, 7%, v/v) was added to an aqueous solution of acetic acid (1%, v/v). The mixed solution was continuously stirred at $60\text{ }^\circ\text{C}$ for 4 h to obtain a yellow viscous solution. Then, the solution was centrifuged at 10 000 rpm for 30 min to separate undissolved large particles. A defined amount of particle-free casting solution was coated on a Teflon-coated dish and dried in an oven at

40 °C overnight. The dried membrane was soaked into 0.1 M sodium hydroxide solution to neutralize the residual acetic acid and then washed gently in distilled water. After washing, the membrane was dried at room temperature. ii) Fabrication of Au NFs electrode: PVA aqueous solution with a concentration of 10 wt% was prepared by mixing PVA powder (molecular weight, 80 000) with deionized water. The mixture was stirred at a temperature of 30 °C for 36 h with a magnetic stirrer at a speed of 400 rpm to obtain a homogeneous solution. Subsequently, the PVA aqueous solution was put into a 10 ml commercial syringe with a steel G22 needle, and the injection rate was 0.4 mL h⁻¹. A high voltage of 15 kV was applied between the needle and collectors at a distance of 10 cm. The randomly oriented PVA nanofibers can be obtained by electrospinning. Then, a layer of gold (\approx 200 nm) was plated onto the surface of the PVA nanofibers via magnetron sputtering (PVD 75 Kurt J. Lesker, Ar, 4 mTorr, 100 W, 15 min) to form uniform conductive PVA/Au NFs. Finally, the metallic PVA/Au NFs were placed on the surface of the water to dissolve PVA. iii) Integration: After drying, Au NFs electrode was transferred to CS substrate. Then, another CS membrane was covered on the top layer of Au NFs.

Sweat Permeability Test: According to the modified American Society for Testing Materials (ASTM) E96 cup standard, the sweat permeability test was quantitatively conducted. The artificial sweat was prepared according to ISO 3160–2 standard, including 20 g L⁻¹ sodium chloride (NaCl), 17.5 g L⁻¹ ammonium chloride (NH₄Cl), 5 g L⁻¹ urea, 2.5 g L⁻¹ acetic acid (CH₃COOH), 15 g L⁻¹ lactic acid, 80 g L⁻¹ sodium hydroxide (NaOH) for adjusting the pH value to 4.7, and DI water. Open glass bottles containing 10 g artificial sweat were sealed by various covers (CS membrane, commercial 3M sealing membrane, PDMS, PE, fabric, and open state). All the samples were placed in an incubator with constant temperature and humidity (37 °C, 40% RH). The daily sweat loss was recorded regularly.

Measurement of Electrical Performance: First, the e-skin with an area of 3 cm × 3 cm is fixed on the fixture with the force sensor. Then, the contact materials (PTFE (thickness 0.1 mm) or weight (2–50 g)) move in contact and separation with the e-skin. At the same time, the electrical signal can be measured by an electrometer, collected by a data acquisition card, and finally displayed on a computer.

In Vitro Degradation Test: Two types of films were prepared for degradation test, which were CS and CS/Au NFs membranes. The dimensions of all the samples were fixed as 2 cm × 2 cm. Each sample was put in a Petri dish with a diameter of 8 cm, which was then filled with 10 mL degradation solutions, including acetic acid (1% v/v, pH 5), peptidase aqueous solution (1 wt%), and hydrogen peroxide aqueous solution (2 wt%). The photos of samples were recorded in different periods.

Characterization and Measurements: UV-vis spectra (UV-3600 Shimadzu) were employed to characterize the optical transparency of samples. FTIR (VERTEX80v, Brucker) spectrometer and XRD (Xper3 power) were used to measure the infrared spectra and the crystalline structure of samples. Mechanical tensile behaviors were conducted using an ESM301/Mark-10 tester under a constant speed of 10 mm s⁻¹. The mechanical tensile tests were performed on a universal material tester (Instron, EP3000). The static water contact angle of the membranes was performed by a contact angle analyzer (SL200B, Kino). Sweat vapor transmission rate was measured by means of a modification of ASTM Method E 96-95 (ASTM, 1995b). The weights of the cups were recorded every hour to calculate the artificial sweat vapor transmission rate and an average value was obtained. The surface morphology and elemental components of the samples were characterized by a field emission scanning electron microscope (Hitachi SU8020) equipped with EDX. As for the electrical characteristics, including output voltage, short-circuit current, and transferred charge, a high-impedance electrometer (6514 Keithley) was used. The periodic contact and separation movements were applied by a commercial linear mechanical motor (LinMot E1100). The applied force was detected by a compression dynamometer (Vernier LabQuest Mini). The software platform was constructed on the basis of LabVIEW.

Statistical Analysis: One-way analysis of variance with the Tukey post hoc test was performed on experiments with more than two test groups.

Continuous variables were expressed as mean \pm standard deviation (SD). *p*-Values < 0.05 were considered significant. All statistical analysis and graphing were performed with Excel software.

Experiments on Human Subjects: All experiments on human skin were carried out under approval from the one subject and first author of the paper. The research was conducted with informed signed consent from the subject. According to the standard, formal approval for this study from the university authorities was not required.

Supporting Information

Supporting Information is available from the Wiley Online Library or from the author.

Acknowledgements

X.P., K.D., and Y.Z. contributed equally to this work. The authors are grateful for the support received from the Minister of Science and Technology (Grant Nos. 2016YFA0202701 and 2016YFA0202703), the Beijing Municipal Natural Science Foundation (Grant No.2212052), and the University of Chinese Academy of Sciences. No formal approval for the experiments involving human volunteers was required. The volunteers took part following informed consent.

Conflict of Interest

The authors declare no conflict of interest.

Data Availability Statement

The data that support the findings of this study are available from the corresponding author upon reasonable request.

Keywords

biodegradable, chitosan, electronic skin, permeable, transparent, triboelectric nanogenerators

Received: November 30, 2021

Revised: December 27, 2021

Published online:

- [1] M. L. Hammock, A. Chortos, B. C. Tee, J. B. Tok, Z. Bao, *Adv. Mater.* **2013**, *25*, 5997.
- [2] C. M. Boutry, A. Nguyen, Q. O. Lawal, A. Chortos, S. Rondeau-Gagne, Z. Bao, *Adv. Mater.* **2015**, *27*, 6954.
- [3] X. Peng, K. Dong, C. Ning, R. Cheng, J. Yi, Y. Zhang, F. Sheng, Z. Wu, Z. L. Wang, *Adv. Funct. Mater.* **2021**, *31*, 2103559.
- [4] K. Dong, Z. Wu, J. Deng, A. C. Wang, H. Zou, C. Chen, D. Hu, B. Gu, B. Sun, Z. L. Wang, *Adv. Mater.* **2018**, *30*, 1804944.
- [5] X. Wang, L. Dong, H. Zhang, R. Yu, C. Pan, Z. L. Wang, *Adv. Sci.* **2015**, *2*, 1500169.
- [6] J. C. Yang, J. Mun, S. Y. Kwon, S. Park, Z. Bao, S. Park, *Adv. Mater.* **2019**, *31*, 1904765.
- [7] S. Bauer, S. Bauer-Gogonea, I. Graz, M. Kaltenbrunner, C. Keplinger, R. Schwodauer, *Adv. Mater.* **2014**, *26*, 149.
- [8] A. Chortos, J. Liu, Z. Bao, *Nat. Mater.* **2016**, *15*, 937.

- [9] Y. Hao, X. He, L. Wang, X. Qin, G. Chen, J. J. A. F. M. Yu, *Adv. Funct. Mater.* **2021**, 2109790.
- [10] H. Guan, T. Zhong, H. He, T. Zhao, L. Xing, Y. Zhang, X. Xue, *Nano Energy* **2019**, 59, 754.
- [11] G. Yang, Y. Tang, T. Lin, T. Zhong, Y. Fan, Y. Zhang, L. Xing, X. Xue, Y. Zhan, *Nano Energy* **2022**, 93, 106817.
- [12] W. Zhang, H. Guan, T. Zhong, T. Zhao, L. Xing, X. Xue, *Nano-Micro Lett.* **2020**, 12, 105.
- [13] D. H. Ho, Q. Sun, S. Y. Kim, J. T. Han, D. H. Kim, J. H. Cho, *Adv. Mater.* **2016**, 28, 2601.
- [14] S. C. Mannsfeld, B. C. Tee, R. M. Stoltenberg, C. V. Chen, S. Barman, B. V. Muir, A. N. Sokolov, C. Reese, Z. Bao, *Nat. Mater.* **2010**, 9, 859.
- [15] X. Wang, Y. Gu, Z. Xiong, Z. Cui, T. Zhang, *Adv. Mater.* **2014**, 26, 1336.
- [16] X. Wang, W. Z. Song, M. H. You, J. Zhang, M. Yu, Z. Fan, S. Ramakrishna, Y. Z. Long, *ACS Nano* **2018**, 12, 8588.
- [17] U. Khan, T. H. Kim, H. Ryu, W. Seung, S. W. Kim, *Adv. Mater.* **2017**, 29, 1603544.
- [18] X. Peng, K. Dong, C. Ye, Y. Jiang, S. Zhai, R. Cheng, D. Liu, X. Gao, J. Wang, Z. L. Wang, *Sci. Adv.* **2020**, 6, eaba9624.
- [19] T. Zhao, Y. Han, L. Qin, H. Guan, L. Xing, X. Li, X. Xue, G. Li, Y. Zhan, *Nano Energy* **2021**, 85, 106006.
- [20] Z. L. Wang, *Faraday Discuss.* **2015**, 176, 447.
- [21] K. Dong, X. Peng, Z. L. Wang, *Adv. Mater.* **2020**, 32, 1902549.
- [22] Z. Wu, T. Cheng, Z. L. Wang, *Sensors* **2020**, 20, 2925.
- [23] Z. L. Wang, J. Chen, L. Lin, *Energy Environ. Sci.* **2015**, 8, 2250.
- [24] K. Dong, X. Peng, J. An, A. C. Wang, J. Luo, B. Sun, J. Wang, Z. L. Wang, *Nat. Commun.* **2020**, 11, 2868.
- [25] S. Wang, J. Y. Oh, J. Xu, H. Tran, Z. Bao, *Acc. Chem. Res.* **2018**, 51, 1033.
- [26] S. Chen, L. Sun, X. Zhou, Y. Guo, J. Song, S. Qian, Z. Liu, Q. Guan, E. M. Jeffries, W. Liu, Y. Wang, C. He, Z. You, *Nat. Commun.* **2020**, 11, 1107.
- [27] J. H. Lee, J. S. Heo, Y. J. Kim, J. Eom, H. J. Jung, J. W. Kim, I. Kim, H. H. Park, H. S. Mo, Y. H. Kim, S. K. Park, *Adv. Mater.* **2020**, 32, 2000969.
- [28] Y. Jiang, K. Dong, X. Li, J. An, D. Wu, X. Peng, J. Yi, C. Ning, R. Cheng, P. Yu, Z. L. Wang, *Adv. Funct. Mater.* **2020**, 31, 2005584.
- [29] X. Peng, K. Dong, Z. Wu, J. Wang, Z. L. Wang, *J. Mater. Sci.* **2021**, 56, 16765.
- [30] W. B. Han, J. H. Lee, J. W. Shin, S. W. Hwang, *Adv. Mater.* **2020**, 32, 2002211.
- [31] W. Li, Q. Liu, Y. Zhang, C. Li, Z. He, W. C. H. Choy, P. J. Low, P. Sonar, A. K. K. Kyaw, *Adv. Mater.* **2020**, 32, 2001591.
- [32] E. Guibal, *Prog. Polym. Sci.* **2005**, 30, 71.
- [33] A. R. Nesic, S. I. Seslija, *Food Packaging* **2017**, 19, 637.
- [34] N. Morin-Crini, E. Lichtfouse, G. Torri, G. Crini, *Environ. Chem. Lett.* **2019**, 17, 1667.
- [35] S. Parvez, M. M. Rahman, M. A. Khan, M. A. H. Khan, J. M. M. Islam, M. Ahmed, M. F. Rahman, B. Ahmed, *Polym. Bull.* **2012**, 69, 715.
- [36] H. Liu, J. Mao, K. Yao, G. Yang, L. Cui, Y. Cao, *J. Biomater. Sci., Polym. Ed.* **2004**, 15, 25.
- [37] L. Wang, Z. Lou, K. Wang, S. Zhao, P. Yu, W. Wei, D. Wang, W. Han, K. Jiang, G. Shen, *Research* **2020**, 2020, 8716847.
- [38] J. Li, J. Gao, G. Sui, L. Jia, C. Zuo, Q. Deng, *Mater. Express* **2014**, 4, 491.
- [39] Y. J. Fan, X. Li, S. Y. Kuang, L. Zhang, Y. H. Chen, L. Liu, K. Zhang, S. W. Ma, F. Liang, T. Wu, Z. L. Wang, G. Zhu, *ACS Nano* **2018**, 12, 9326.
- [40] B. Sun, R. N. McCay, S. Goswami, Y. Xu, C. Zhang, Y. Ling, J. Lin, Z. Yan, *Adv. Mater.* **2018**, 30, 1804327.
- [41] C. Wang, T. Yokota, T. Someya, *Chem. Rev.* **2021**, 121, 2109.
- [42] C. M. Boutry, Y. Kaizawa, B. C. Schroeder, A. Chortos, A. Legrand, Z. Wang, J. Chang, P. Fox, Z. Bao, *Nat. Electron.* **2018**, 1, 314.
- [43] S. Chen, J. Xie, J. Liu, X. Huang, C. Wang, *J. Mater. Sci.* **2020**, 56, 2725.
- [44] X. Pu, M. Liu, X. Chen, J. Sun, C. Du, Y. Zhang, J. Zhai, W. Hu, Z. L. Wang, *Sci. Adv.* **2017**, 3, e1700015.
- [45] P. Won, J. J. Park, T. Lee, I. Ha, S. Han, M. Choi, J. Lee, S. Hong, K. J. Cho, S. H. Ko, *Nano Lett.* **2019**, 19, 6087.
- [46] D. J. Lipomi, M. Vosgueritchian, B. C. Tee, S. L. Hellstrom, J. A. Lee, C. H. Fox, Z. Bao, *Nat. Nanotechnol.* **2011**, 6, 788.
- [47] X. Fu, L. Wang, L. Zhao, Z. Yuan, Y. Zhang, D. Wang, D. Wang, J. Li, D. Li, V. Shulga, G. Shen, W. Han, *Adv. Funct. Mater.* **2021**, 31, 2010533.
- [48] S. Lee, E. H. Kim, S. Yu, H. Kim, C. Park, S. W. Lee, H. Han, W. Jin, K. Lee, C. E. Lee, J. Jang, C. M. Koo, C. Park, *ACS Nano* **2021**, 15, 8940.
- [49] Y. Zhang, L. Wang, L. Zhao, K. Wang, Y. Zheng, Z. Yuan, D. Wang, X. Fu, G. Shen, W. Han, *Adv. Mater.* **2021**, 33, 2007890.
- [50] X. Wang, Y. Zhang, X. Zhang, Z. Huo, X. Li, M. Que, Z. Peng, H. Wang, C. Pan, *Adv. Mater.* **2018**, 30, e1706738.
- [51] Y. Zhang, Z. Huo, X. Wang, X. Han, W. Wu, B. Wan, H. Wang, J. Zhai, J. Tao, C. Pan, Z. L. Wang, *Nat. Commun.* **2020**, 11, 5629.
- [52] A. Miyamoto, S. Lee, N. F. Cooray, S. Lee, M. Mori, N. Matsuhisa, H. Jin, L. Yoda, T. Yokota, A. Itoh, M. Sekino, H. Kawasaki, T. Ebihara, M. Amagai, T. Someya, *Nat. Nanotechnol.* **2017**, 12, 907.
- [53] D.-H. Kim, N. Lu, R. Ma, Y.-S. Kim, R.-H. Kim, S. Wang, J. Wu, S. M. Won, H. Tao, A. J. Islam, K. J. Yu, T. Kim, R. Chowdhury, M. Ying, L. Xu, M. Li, H.-J. Chung, H. Keum, M. McCormick, P. Liu, Y.-W. Zhang, F. G. Omenetto, Y. Huang, T. Coleman, J. A. Rogers, *Science* **2011**, 333, 838.
- [54] V. R. Feig, H. Tran, Z. Bao, *ACS Cent. Sci.* **2018**, 4, 337.